



# Study of solar neutrinos with the 600 t liquid argon ICARUS detector

F. Arneodo<sup>a</sup>, A. Badertscher<sup>b</sup>, S. Baibussinov<sup>c</sup>, P. Benetti<sup>d</sup>, A. Borio di Tigliole<sup>e</sup>,  
R. Brunetti<sup>d</sup>, A. Bueno<sup>b</sup>, E. Calligarich<sup>d</sup>, M. Campanelli<sup>b</sup>, C. Carpanese<sup>b</sup>,  
D. Cavalli<sup>f</sup>, F. Cavanna<sup>g</sup>, P. Cennini<sup>h</sup>, S. Centro<sup>c</sup>, A. Cesana<sup>e</sup>, C. Chen<sup>i</sup>, Y. Chen<sup>i</sup>,  
D. Cline<sup>j</sup>, I. De Mitri<sup>a</sup>, R. Dolfini<sup>d,\*</sup>, A. Ferrari<sup>f,h</sup>, A. Gigli Berzolari<sup>d</sup>, P. Goudsmit<sup>b</sup>,  
K. He<sup>i</sup>, X. Huang<sup>i</sup>, Z. Li<sup>i</sup>, F. Lu<sup>i</sup>, J. Ma<sup>i</sup>, G. Mannocchi<sup>k</sup>, M. Maris<sup>l</sup>, F. Mauri<sup>d</sup>,  
D. Mazza<sup>g</sup>, L. Mazzone<sup>d</sup>, C. Montanari<sup>d</sup>, S. Otwinowski<sup>j</sup>, O. Palamara<sup>a</sup>,  
D. Pascoli<sup>c</sup>, A. Pepato<sup>c</sup>, L. Periale<sup>m</sup>, S. Petrer<sup>g</sup>, G. Piano Mortari<sup>g</sup>, A. Piazzoli<sup>d</sup>,  
P. Picchi<sup>k</sup>, F. Pietropaolo<sup>c</sup>, A. Rappoldi<sup>d</sup>, G.L. Raselli<sup>d</sup>, J.P. Revol<sup>h</sup>, M. Rossella<sup>d</sup>,  
C. Rossi<sup>g</sup>, A. Rubbia<sup>b</sup>, C. Rubbia<sup>d,h</sup>, P. Sala<sup>f,h</sup>, D. Scannicchio<sup>d</sup>, F. Sergiampietri<sup>n</sup>,  
S. Suzuki<sup>m</sup>, M. Terrani<sup>e</sup>, S. Ventura<sup>c</sup>, C. Vignoli<sup>d</sup>, H. Wang<sup>l</sup>, J. Woo<sup>l</sup>, G. Xu<sup>i</sup>,  
Z. Xu<sup>i</sup>, C. Zhang<sup>i</sup>, Q. Zhang<sup>i</sup>, S. Zheng<sup>i</sup>

<sup>a</sup>Laboratori Nazionali del Gran Sasso, SS 17 bis - km 18.910, Assergi (AQ), Italy

<sup>b</sup>Eidgenössische Technische Hochschule, CH-8093 Zürich, Switzerland

<sup>c</sup>Dipartimento di Fisica e INFN, Università di Padova, via Marzolo 8, I-35131 Padova, Italy

<sup>d</sup>Dipartimento di Fisica e INFN, Università di Pavia, via Bassi 6, I-27100 Pavia, Italy

<sup>e</sup>Dipartimento di Ingegneria Nucleare del Politecnico di Milano, via Ponzio 34/3, e INFN Sezione di Milano,  
via Celoria 16, I-20133 Milano, Italy

<sup>f</sup>Dipartimento di Fisica e INFN, Università di Milano, via Celoria 16, I-20133 Milano, Italy

<sup>g</sup>Dipartimento di Fisica e INFN, Università dell'Aquila, via Vetoio, I-67010 L'Aquila, Italy

<sup>h</sup>CERN, CH-1211 Geneva 23, Switzerland

<sup>i</sup>Institute of High Energy Physics, 19 Yuquan Road, Beijing, People's Republic of China

<sup>j</sup>Department of Physics, University of California, Los Angeles, CA 90024, USA

<sup>k</sup>Laboratori Nazionali dell'INFN di Frascati, via Fermi 40, I-00044 Frascati (Roma), Italy

<sup>l</sup>Osservatorio Astronomico di Trieste, via G.B. Tiepolo 11, I-34131 Trieste, Italy

<sup>m</sup>ICGF del CNR, Corso Fiume 4, I-10133 Torino, Italy

<sup>n</sup>INFN Sezione di PISA, via Livornese 1291, I-56010 San Piero a Grado (PI), Italy

Received 17 January 2000; received in revised form 13 April 2000; accepted 21 April 2000

---

## Abstract

The ICARUS time projection chamber can yield sound information on <sup>8</sup>B solar neutrinos. Owing to the high-energy resolution and the good capability of event reconstruction it can make a contribution to our understanding of neutrino

---

\* Corresponding author.

E-mail address: rinaldo.dolfini@pv.infn.it (R. Dolfini).

intensities and their energy spectrum. Moreover, the MSW oscillation probability for sterile and active neutrinos can be well studied because both elastic scattering by electrons and absorption reaction on argon nuclei can be measured independently. The main problem in detecting the low-energy neutrino interactions arises from the environmental radioactivity. In the present work we study by Monte Carlo simulation the topology and the rates of the events, induced by neutrinos and background neutrons, in a 470 t (fiducial mass) liquid-argon TPC detector. For neutrino interactions we use the standard solar model BP98 and the recent experimental confirmation of the shell model computation of absorption cross section. The noise is estimated from new data on natural neutron background, collected in the hall C of the Gran Sasso laboratory. It is confirmed that, with a relatively modest neutron shielding and particular off-line event triggers, the weight of spurious events can be made to have little influence on the ICARUS solar neutrino measurement. Indeed, we expect 6 (26) background events per year in the 212 (759) elastic scattering (absorption reaction) sample. © 2000 Elsevier Science B.V. All rights reserved.

PACS: 26.65; 29.40

Keywords: Solar neutrinos; Liquid argon; Detectors

## 1. Introduction

The five solar neutrino experiments (Homestake-chlorine [1], Kamiokande [2], GALLEX [3], SAGE [4] and Super-Kamiokande [5]), make evident a strong suppression of the measured intensities, with respect to the combined predictions of the stellar evolution models and standard electroweak theory, with zero neutrino mass. For instance BP98 [6], which is considered the reference Standard Solar Model, gives for the  $^8\text{B}$  integral flux the following estimation:

$$5.15 \times 10^6 (1.00^{+0.19}_{-0.14}) \text{ cm}^2 \text{ s}^{-1} (\text{SSM BP98}).$$

Compared to this prediction the intensity lack measured by Super-Kamiokande is

$$\frac{\text{Data}}{\text{SSM BP98}}$$

$$= 0.474^{+0.010}_{-0.009} (\text{stat.})^{+0.017}_{-0.014} (\text{syst.})^{+0.090}_{-0.066} (\text{BP 98}).$$

Another interesting outcome is the anomaly of the electron recoil energy reported by the Super-Kamiokande measurement. The ratio of the measured to the calculated number of events as a function of the electron recoil energy increases above 13 MeV. A possible contribution of the hep process has been claimed to explain this surprising effect [7,8].

The Homestake-chlorine neutrino experiment has been yielding coherent results over 30 years of

operation; the GALLEX and SAGE experiments are based on the same detection mechanism and are directly calibrated with artificial neutrino sources; Super-Kamiokande is a replica on a larger scale of the Kamiokande experiment and is indirectly calibrated with an electron accelerator. These considerations lead some people to exclude unknown experimental systematic errors. All the proposed solar models are in fair agreement with the experimental observations concerning the solar structure as is the case, for instance, of helioseismology, but fail to explain at the same time the solar neutrino problem (SNP). Hence the significant suppression of the solar  $\nu_e$  flux seems to provide definite evidence of new physics beyond the minimal standard model for electroweak interactions.

Vacuum oscillations and the MSW effect for active and sterile neutrinos, are among the most promising hypotheses able to explain the lack of neutrinos. Nevertheless a satisfactory interpretation of the experimental observations has not yet been reached even considering the results of other neutrino experiments such as CHOOZ [9]. A determination of the solar neutrino spectral shape could give a sound contribution to the understanding of the true mechanism responsible for the neutrino deficit.

The ICARUS T600 detector has some unique peculiarities. The first module will be mounted and tested before the end of 2000 [10]. It has a mass which is only 2.1% of Super-Kamiokande, but its

higher intrinsic efficiency, the very good energy resolution, and the detailed description of each event (which allows to recognise scattering and absorption interactions) reduces the gap between the event rates to a factor less than 10. This detector offers the possibility to obtain accurate information on the high-energy region (above 5 MeV) of the solar neutrino spectrum and to put a constraint on the contribution of the hep process. We note that in the region between 10 and 19 MeV, where the hep spectrum dominates, the ICARUS detector offers an optimal track reconstruction of energy and direction. Moreover, in this energy region there is neither background from natural radioactivity nor contamination from atmospheric neutrinos.

The present work is an updating of a previous paper in which we studied the topology and the rates of the solar neutrino events, including the effect of the radioactivity of the rocks in hall C of the Gran Sasso Laboratories (LNGS) [11]. The BP98 standard solar model together with recent measurements of the  $^{40}\text{Ti}$   $\beta^+$  decay [12] and new data collected in hall C on the neutron natural background [13] have been used to update the previous predictions. It is stated that an adequate number of events should be collected in a reasonable time and that neutrons are the main source of noise. From the simulations it appears that with a convenient choice of off-line trigger and neutron shielding the weight of spurious events can be made to be shown to have no influence in practice. The programs GEANT, MCNP and FLUKA were used for the simulations [14–16].

## 2. ICARUS T600 detector

The detector internal volume consists of two half-modules filled with liquid argon (LAr). The dewar is surrounded by a 0.6 m thick aluminium and paper honeycomb which acts as thermal insulator. The total dewar mass is about 50 t. We plan to shield the top and the sides of the detector against neutrons with a 70 cm thick layer of polyethylene tubes filled with boric acid. The sensitive volume of each half-module is seen by two Time Projection Chambers (TPC) with a common cathode located along the central longitudinal plane

and the readout is made with three wire planes at the lateral sides (see Fig. 1). The main parameters of the chambers are summarised in Table 1.

The ICARUS detector will detect the neutrinos via the elastic scattering by electrons and the absorption reaction by  $^{40}\text{Ar}$  nuclei. These interactions usually result in the production of a primary electron track sometimes surrounded by lower-energy secondary electron tracks.

Small prototypes have demonstrated that, by the TPC technique, electrons with kinetic energy as low as 150 keV can be detected [17]. This performance allows a detailed reconstruction of the neutrino interactions. The background induced by natural radioactivity and the need to establish the electron direction in elastic scattering events require a threshold for the detection of primary electrons. As will be discussed below, this threshold is of the order of 5 MeV for elastic and absorption events.

## 3. Event rate evaluations

These computations are performed by means of the MCNP program. The LNGS hall C is approximated by a parallelepiped 20.6 m wide, 9 m high and 100 m long, surmounted by a half-cylinder of radius 10.3 m. The ICARUS detector is simulated according to the scheme described above and is located in the corner near the main entrance of the hall. For the computation we consider the following regions: an external neutron shielding layer, a thermal insulating material cavity, a liquid argon dead layer 0.35 m thick, and the sensitive volume divided into 48 identical cells. The purpose of the computations is to derive the background event topology and the frequency and energy distribution of the resulting electron tracks in the sensitive volume.

### 3.1. Background sources

The following background sources were considered:

(a) *Natural radioactivity*: The decay of  $^{40}\text{K}$ , uranium, thorium, radon and daughters, present in the rock or in the atmosphere surrounding the detector, generate photons and can produce neutrons by spontaneous fission (SF) or ( $\alpha$ ,n) reactions. The

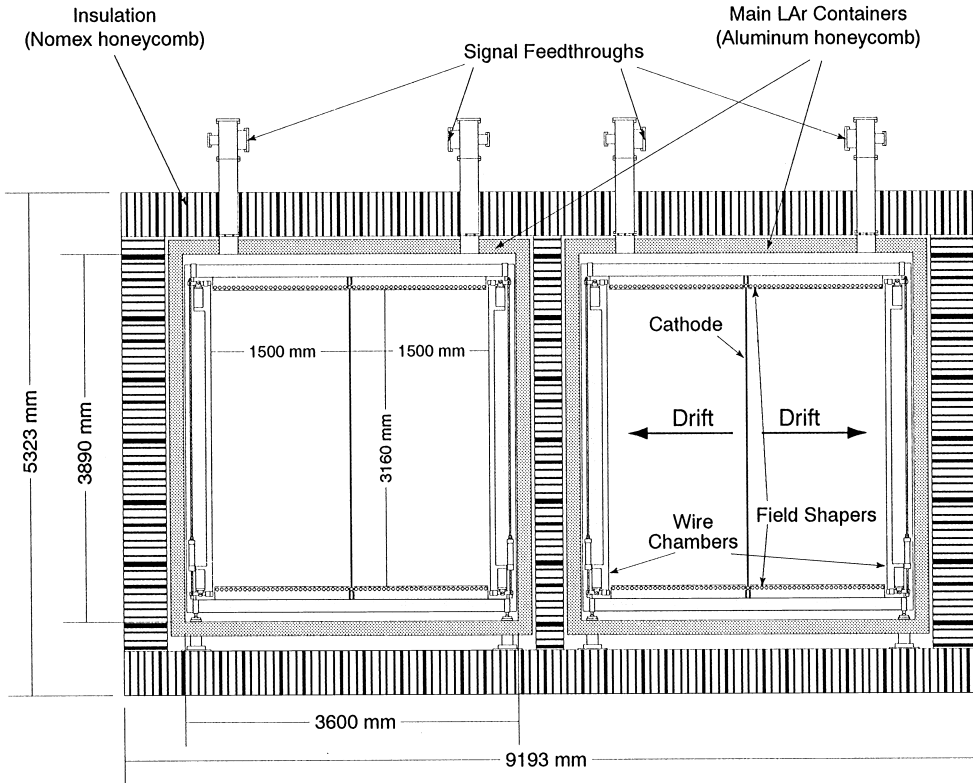


Fig. 1. Drawing of the ICARUS T600 detector.

Table 1  
Main parameters of the readout chambers of the ICARUS detector

Number of readout chambers	4
Number of sensitive wire planes	3
Wire orientation with respect to the horizontal	0°, ± 60°
Wire pitch	3 mm
Maximum drift length	1.5 m
Maximum drift time at 500 V/cm	1.0 ms
Sensitive volume/chamber	85.1 m <sup>3</sup>
Length	17.95 m
Width	1.5 m
Height	3.16 m
Total sensitive volume (4 chambers)	340 m <sup>3</sup>
Total sensitive LAr mass	470 ton

rock surrounding the cavern is assumed to be limestone [18] with a mean density of 2.8 g cm<sup>-3</sup>, a potassium concentration of 0.33% [19], and an

uranium and thorium specific activity of 1.7 and 1.9 Bq kg<sup>-1</sup>, respectively [20]. From the <sup>40</sup>K decay, 1.46 MeV photons are produced at a rate of 3250 photons per second per kilogram of natural potassium. Supposing uranium and thorium chains were at equilibrium, 1.98 and 2.48 photons are emitted, respectively, for each uranium and thorium disintegration. The energy spectrum of these photons extends up to 2.6 MeV. Considering the radioactive nuclide concentrations quoted above we expect that about 2 × 10<sup>7</sup> s<sup>-1</sup> kt<sup>-1</sup> photons of various energies will be generated in the rock. Photons can also be produced by neutron capture in the rock but in an amount of several orders of magnitude lower. Among natural nuclides, SF is important only for <sup>238</sup>U. Assuming for uranium the specific activity quoted above, T<sub>1/2</sub>(SF) = 8.2 × 10<sup>15</sup> yr, T<sub>1/2</sub>(α) = 4.5 × 10<sup>9</sup> yr and 2 neutrons per fission [21], we obtain a neutron production of 1.87 s<sup>-1</sup> kt<sup>-1</sup>. In most of the minerals uranium is present in an oxide form, hence oxygen is probably

the main element involved in neutron production by ( $\alpha$ ,n) reactions. Assuming that uranium is at the equilibrium with 7 daughter alpha-emitters and thorium with 5 daughter alpha-emitters, and that all these nuclides have the same neutron yield of  $6.5 \times 10^{-8}$  neutrons per alpha-particle [22], we have a neutron production of  $1.63 \text{ s}^{-1} \text{ kt}^{-1}$ .

(b) *Radioactive pollution in liquid argon*: Natural argon could contain small amounts of  $^{39}\text{Ar}$  and  $^{42}\text{Ar}$ . The second, which is by far the most important source of background, is supposed to be present with a concentration of  $7 \times 10^{-22}$  atoms of  $^{42}\text{Ar}$  per natural Ar atom [23].

(c) *Radioactivity of structural materials*: The materials constituting the dewar walls (honeycomb panels) have been analysed for radioactive contamination. From the analyses we found an upper limit for both uranium and thorium at about 0.04 ppm. In these limits we expect 0.045 neutrons per second from the whole dewar material. This is more than one order of magnitude lower than the rate due to the rock contamination.

(d) *Nuclear photo-dissociation*: In addition to the natural radioactivity, the high-energy muons which penetrate the rock, can induce nuclear photo-dissociation. The neutron production rate in the rock was estimated to be about  $9 \times 10^{-3} \text{ s}^{-1} \text{ kt}^{-1}$  [24]. Since this figure is about two orders of magnitude lower than the previous ones this way of production is relatively unimportant. Besides, the interaction of a neutron generated in LAr by a muon crossing the sensitive volume, is accompanied by the muon track and can then be easily recognised.

From these considerations it follows that the natural radioactivity of the rocks is by far the most important background component, hence it was the only radiation source considered. Particular care was devoted to neutrons which are the only radiation able to generate high-energy electrons in the most significant energy range of the  $^8\text{B}$  neutrino spectrum to be searched for by the ICARUS apparatus.

### 3.2. Event rates and energy threshold computations

We determined the intensity and energy distribution of electron tracks produced in the sensitive volume.

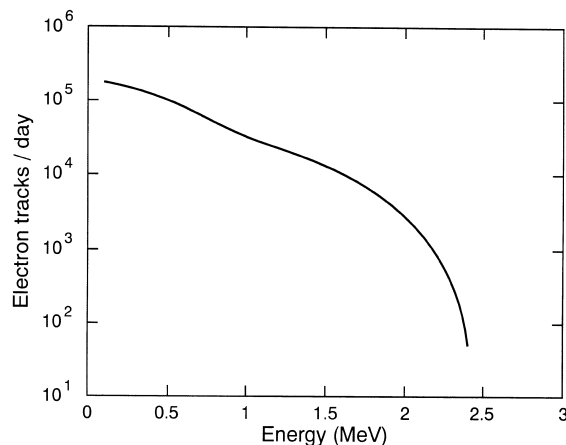


Fig. 2. Integral electron track energy spectrum generated from photon interaction.

#### 3.2.1. Background intensity

The radiation sources were obtained from measured photon [25] and neutron [13] spectra in the hall, which were assumed to be a projection of the spectra of the particles emerging from the rocks. Photons and neutrons were considered independently.

(a) *Photons*: In the two external TPC chambers (see Fig. 1)  $1.8 \times 10^5$  electron tracks/day are foreseen. Going towards the detector centre the track density decreases by more than one order of magnitude. The mean energy distribution of electron tracks in the detector is shown in Fig. 2. No electron tracks are expected with energy greater than 2.4 MeV. Each event consists of a main track possibly surrounded by electrons produced by the interaction of bremsstrahlung photons. The distribution of these events according to the energy of the most energetic electron track is displayed in the fifth column of Table 2.

(b) *Neutrons*: As said above, neutron-capture gamma rays produce electron tracks which can simulate all the possible neutrino interactions. The scope of the computations is to evaluate the background intensities for each class of true events: elastic scattering and absorption. The computation is performed in two steps. First we calculate the neutron capture intensity and then we estimate the abundance of the events generated by the gamma

Table 2

Events per year and for 470 t liquid argon detector as a function of the kinetic energy threshold  $T_{\text{th}}$ 

$T_{\text{th}}$ (MeV)	Events/year				
	Elastic	Fermi	Gamow–Teller	Photons	Neutrons
0.0000	1257	923	894	6.5700e + 07	7400
1.0000	1052	906	894	1.1801e + 07	3404
2.0000	858	842	878	1.0056e + 06	1554
3.0000	676	719	861		696
4.0000	513	541	800		318
5.0000	372	343	683		144
5.5000		249	514		
6.0000	254	167	326		66
6.5000		100	237		
7.0000	163	52	159		30
7.5000		22	96		
8.0000	96	7	50		13
8.5000		2	21		
9.0000	50		7		
9.5000			2		
10.000	23				

rays, classified according to their nature (number of electron tracks, energy, etc.). In the shielded detector the captures occur mostly in LAr. Each of the four TPCs, which constitute the detector, is split into 12 equal cells in which the mean neutron capture rate per unit injected neutron is estimated by the MCNP program. We use as input the neutron spectrum resulting from our measurement in the Gran Sasso laboratory hall C, which is assumed to be a projection of the neutron spectrum at the surface of the hall. Simultaneously the neutron flux intensity is computed at a point of the hall far from the detector. By comparing computations at this point and measurements we obtain the normalisation factor, i.e., the number of neutrons injected in the hall per second. The result is  $12 \text{ s}^{-1}$ , which is in fair agreement with the results of simulation considering the uranium and thorium contamination of the rocks. The resulting capture intensities are nearly the same in the four chambers, respectively:  $6.6 \times 10^{-5} \text{ s}^{-1}$ ,  $5.0 \times 10^{-5} \text{ s}^{-1}$ ,  $5.3 \times 10^{-5} \text{ s}^{-1}$  and  $6.5 \times 10^{-5} \text{ s}^{-1}$ . Hence we expect about 7400 captures per year in the 470 t fiducial mass. Neutron capture events in LAr are then simulated by the GEANT program. Each event consists of a number of tracks produced by de-excitation or by brems-

strahlung photons. The distribution of these events according to the energy of the most energetic electron track is displayed in the last column of Table 2.

### 3.2.2. Intensity of neutrino events

We consider separately neutrino elastic scattering (ES), neutrino capture to the 4.38 MeV Isotopic Analogue State (IAS) of  $^{40}\text{K}$ , which is a Fermi transition (FT), and Gamow–Teller transitions (GT) to several  $^{40}\text{K}$  levels [26]. The  $^8\text{B}$  solar neutrino flux is the one foreseen by the BP98 standard solar model.

The elastic scattering event rate at different values of the cutoff kinetic energy of the recoil electron is computed by using the cross-section values taken from Ref. [27]. For neutrino capture, the shape of the cross-section (evaluated for transition to the IAS) is assumed to be the same for Fermi and Gamow–Teller transitions and the absolute values are computed by normalisation to the theoretical values obtained by shell model calculations [26].

The Fermi and Gamow–Teller contributions to the neutrino absorption on  $^{40}\text{Ar}$  can be obtained indirectly also from the measurements of  $\beta^+$  decay

Table 3  
Neutrino cross-sections as a function of the minimum accepted kinetic energy ( $T_{\text{th}}$ )

$T_{\text{th}}$ (MeV)	Neutrino absorption cross-section ( $10^{-43}$ cm $^2$ )		
	Elastic	Fermi	Gamow–Teller
0	0.608	8.08	16.10
1	0.509	7.93	15.80
2	0.415	7.34	14.60
3	0.327	6.26	12.40
4	0.248	4.72	9.40
5	0.180	2.99	5.94
6	0.123	1.45	2.89
7	0.079	0.46	0.91
8	0.0464	0.06	0.12
9	0.0244		
10	0.0110		

of the mirror nucleus  $^{40}\text{Ti}$ , assuming isospin symmetry. Two recent experiments give slightly discrepant results. One of them, described in Ref. [12], yields cross-section values somewhat greater, while the second [28] substantially confirms the theoretical predictions. The summary is shown in Table 3.

In order to be conservative we decided to use the lowest cross-section values. The resulting neutrino interaction intensities are summarised in columns 2–4 of Table 2.

### 3.2.3. Fractional statistical error

Combining all the data (background and true event intensities) we compute the fractional statistical error on neutrino events expected in 1 year of data taking as a function of the kinetic energy cut on the most energetic electron, as shown in Fig. 3. A large plateau is evident in the 3–5 MeV interval. In order to study the neutrino energy spectrum, it could be convenient to assume the lowest threshold possible, but other considerations, such as the measurements of the electron track direction in the elastic scattering, suggest the use of the greatest cut value in the plateau region. Hence we chose the 5 MeV value.

The topologies of the neutron capture events in which at least one electron has kinetic energy greater than 5 MeV, obtained with the GEANT program, are displayed in Table 4. Here the frac-

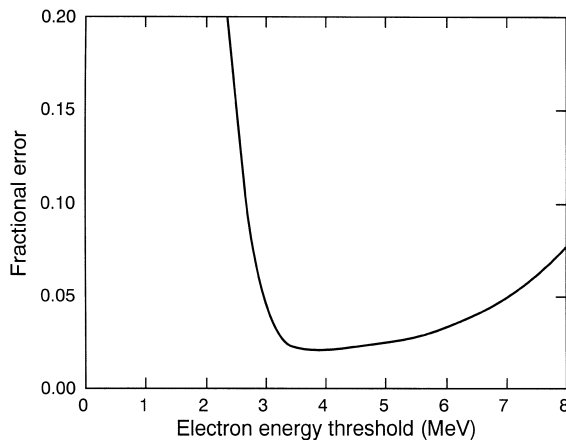


Fig. 3. Fractional statistical error on total neutrino events collected in one year data taking vs. the main electron energy threshold.

Table 4

Fraction of neutron capture events with at least one electron with kinetic energy greater than 5 MeV as a function of the associated energy and Compton electron multiplicity

Associated energy (MeV)	Electron multiplicity			
	0	1	2	> 2
$E < 1$	0.46	0.26	0.10	0
$E \geq 1$	0	0.05	0.07	0.06

tion of events is shown as a function of the associated energy and Compton electron multiplicity. This table together with the values displayed in the last column of Table 2 will allow the computation of the background contamination in each class of events.

## 4. Neutrino simulations

The  $^8\text{B}$  neutrinos are generated according to the theoretical spectrum and we reconstruct their interactions (elastic and absorption type) inside the liquid argon fiducial volume. The GEANT program performs the transport of gamma rays and electrons inside the liquid argon. Every

electron track is then digitised by the following procedure:

- the deposited energy is converted in charge;
- the charge is drifted towards the electrodes with an infinite electron life time in LAr;
- digitised electronic signals are generated on three wire planes placed at  $60^\circ$  from one another, with 3 mm wire pitch;
- Gaussian distributed electronic noise is added with zero mean value and 1000 electrons standard deviation. The resulting electron threshold, which is strongly correlated with electronic noise and with the sense wire pitch, is 150 keV;
- the digitised signals are picked up from the noise by means of an integral-differential algorithm;
- the final parameters (position and energy after digitisation) are obtained by a fitting procedure of the signals.

A Monte Carlo absorption event is shown in Fig. 4. It is characterised by the track of the primary electron generated in the interaction, surrounded by a number of secondary tracks produced by

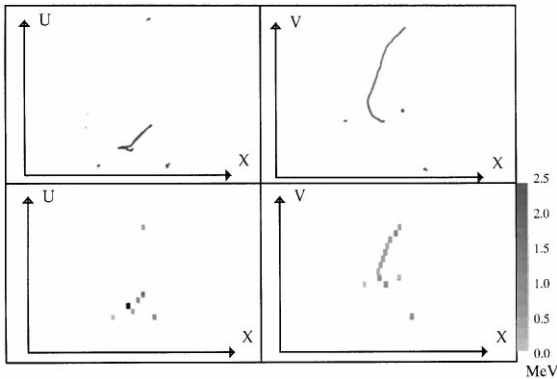


Fig. 4. In the top an absorption event as generated by the GEANT Monte Carlo program is shown in two wire planes ( $U$  and  $V$  coordinates) put at an angle of  $60^\circ$ , the  $X$ -axis is the drift coordinate. The projected track length is about 3 cm, the main electron energy is 7 MeV, the associated energy is 2 MeV and the associated multiplicity is 3. In the bottom the same event is shown after digitisation. The grey scale of each pixel is proportional to the deposited charge. The resolution in the horizontal axis (drift direction) is 0.1 mm, and in the vertical axis is 3 mm (wire pitch).

photons following the  $^{40}\text{K}^*$  de-excitation. The simulations show that the probability of finding the secondary electron tracks vanishes 50 cm away from the interaction point.

The electron suffers strong multiple scattering and bremsstrahlung. The deviation from the straight line decreases with increasing energy. In the majority of cases it is possible to reconstruct at least the track direction for energies greater than 5 MeV, in agreement with previous statistical considerations.

In summary, the signature of a solar neutrino interaction is one electron track, with energy greater than the threshold value, eventually associated to lower energy tracks contained in a 50 cm radius sphere around it. The correlation between associated multiplicity and energy will be used to define the off-line event triggers and to evaluate the trigger efficiencies  $\varepsilon_{\text{ES}}$ ,  $\varepsilon_{\text{GT}}$  and  $\varepsilon_{\text{FT}}$  for scattering and absorption channels.

#### 4.1. Elastic scattering

$$\nu_{e,\mu,\tau} + e^- \rightarrow \nu_{e,\mu,\tau} + e^-.$$

The electron produced via an elastic scattering has an angular distribution, with respect to the initial solar neutrino direction, strongly peaked in the forward direction and we use this signature to discriminate neutrino events from background. In Fig. 5 is shown the fraction of events ( $E > 5$  MeV) as a function of the angle between the scattered electron and the parent solar neutrino direction. For instance if one chooses the tracks within a  $25^\circ$  cone around the sun-detector direction, the angular efficiency is 65%.

The fraction of the events as a function of the associated multiplicity and energy of the secondary tracks is shown in Table 5.

It is very important to reconstruct the main vertex of the scattered electron for this kind of events. If this were not the case, the background should be multiplied by a factor two. In our computations the first hit wire can be distinguished from the end point of one electron with an efficiency greater than 80%. We choose as starting point of the electron, the wire (between the two extreme hit wires) having the lower deposited energy. In fact the wire near the

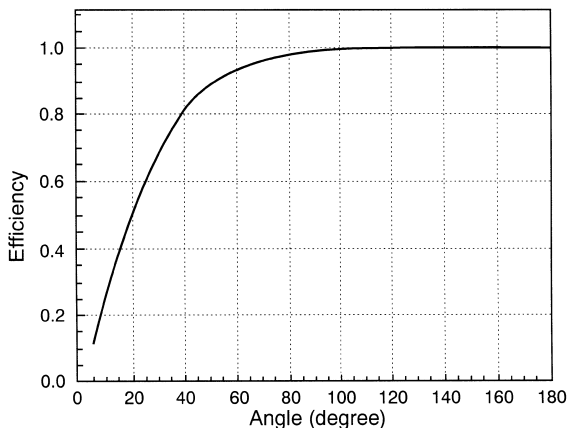


Fig. 5. Fraction of elastic events ( $E > 5$  MeV) as a function of the cone angle within which the reconstructed electron direction in space is contained; the cone axis is defined by the parent neutrino direction. Three wire planes put at  $60^\circ$  angle and a 3 mm wire pitch are used.

Table 5

Fraction of neutrino elastic scattering events as a function of the associated energy and multiplicity. The data obtained after digitisation are used

Associated energy (MeV)	Electron multiplicity			
	0	1	2	3
$E < 1$	0.880	0.073	0.008	0
$E \geq 1$	0	0.015	0.015	0.009

end point, owing to the increase in multiple scattering, collects usually more charge than the one close to the main vertex.

We assume the following constraints as definition of the off-line trigger:

- (1) primary electron energy greater than 5 MeV;
- (2) the cone aperture around the real emission direction of the electron is  $25^\circ$  (efficiency  $\varepsilon_1 = 0.65$ );
- (3) the associated multiplicity is 0 (efficiency  $\varepsilon_2 = 0.88$ , see Table 4).

The total detection efficiency is  $\varepsilon_{ES} = 0.572$ . The total elastic event expected rate will be about 212 per year (see Table 4). The contamination of neutron capture events is 144 events/year (see Table 2),

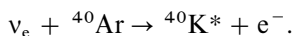
Table 6

Fraction of Gamow–Teller events as a function of the associated energy and multiplicity. The data obtained after digitisation are used

Associated energy (MeV)	Electron multiplicity			
	0	1	2	$\geq 3$
$0 \geq E < 1$	0.083	0.168	0.049	0
$E \geq 1$	0	0.075	0.297	0.328

which reduces to  $144 \times 0.46 = 66$  events simulating elastic scattering (see Table 4). The number is further reduced to 4.7% by the angular cut (which becomes 9.4% if we are not able to determine the electron direction of flight). Hence, in this conservative hypothesis, we expect 6 background events/year in the shielded detector.

#### 4.2. Absorption events



The angular distributions of electrons exhibit a broad peak at about  $120^\circ$  and  $60^\circ$  for the Gamow–Teller and Fermi events, respectively [26], but the measured distributions are flattened because of the digitisation, so that, to a first approximation electron track directions can be considered isotropically distributed.

##### 4.2.1. Allowed Gamow–Teller transitions

In Table 6 the correlation between the associated multiplicity and secondary electron total energy is shown. We assume the following constraints as definition of the off-line trigger:

- (1) primary electron kinetic energy greater than 5 MeV;
- (2) associated energy  $E \geq 1$  MeV,  $\varepsilon_{GT} = 0.70$  (see Table 6).

The final expectation will be about 478 events/year.

##### 4.2.2. Super allowed Fermi transition

In Table 7 the correlation between the associated multiplicity and energy is shown. We assume the

Table 7

Fraction of pure Fermi events as a function of the associated energy and multiplicity. The data obtained after digitisation are used

Associated energy (MeV)	Electron multiplicity			
	0	1	2	$\geq 3$
$E < 1$	0.032	0.039	0.018	0
$E \geq 1$	0	0.081	0.221	0.519

following constraints as definition of the off-line trigger:

- (1) primary electron kinetic energy greater than 5 MeV,
- (2) associated energy  $E \geq 1$  MeV,  $\varepsilon_{\text{FT}} = 0.82$  (see Table 7).

The final expectation will be 281 events/year.

The total absorption rate will be about 759 events/year with a contamination from neutron captures of 26 events/year (see Tables 2 and 4 with the following requirement: associated energy  $E \geq 1$  MeV, multiplicity  $\geq 1$ ). 8.3% of Gamow–Teller and 3.2% of Fermi-type events can simulate the elastic scattering sample. Taking into account the angular cut this means a contamination of no more than 5 events/year in the elastic scattering sample, while the contamination from elastic into absorption sample is 3.9%, i.e., 8 events/year.

## 5. Conclusion

We summarise the results in Table 8, where the estimated rates of events per year are shown together with the background rate. From this table we conclude that a clean measure of  ${}^8\text{B}$  solar neutrinos can be performed in a reasonable data-taking time. It is important to bear in mind that this is possible because of the low intensity of background signals. Noise is mainly related to the neutron flux level in the LNGS laboratories and to the concentration of contaminants (especially uranium) in the materials which will be used for the detector construction. Little more can be done to reduce the neutron flux. The choice of the materials must be

Table 8

Expected number of events per year compared with the computed background rate. The numbers of events must be reduced by a factor  $\approx 0.5$ , if we take into account the solar neutrino deficit revealed by experiments [5]

	Events/year
Elastic channel ( $E \geq 5$ MeV)	212
Background	6
Absorption event contamination	5
Absorption channels	759
Background	26
Elastic event contamination	8

accurate, but purity requirements are within the values specified for industrial products which can easily be found on the market.

## Appendix A. Mixing variables allowed regions

Hence Super-Kamiokande confirms the lack of  $\nu_e$  in the  ${}^8\text{B}$  neutrino flux and presents the following allowed regions for the  $\nu_e \rightarrow \nu_{\mu,\tau}$  MSW oscillation centred in the mixing variables:

SMA, Small Mixing Angle:  $\sin^2 2\theta \approx 5.5 \times 10^{-3}$ ,  $\Delta m^2 \approx 5.4 \times 10^{-6} \text{ eV}^2$

LMA, Large Mixing Angle:  $\sin^2 2\theta \approx 0.76$ ,  $\Delta m^2 \approx 1.8 \times 10^{-5} \text{ eV}^2$

LOW, low probability low mass:  $\sin^2 2\theta \approx 0.96$ ,  $\Delta m^2 \approx 7.9 \times 10^{-8} \text{ eV}^2$ .

The three scenarios for the MSW effect: SMA, LMA and LOW solutions are considered in Fig. 6, where the  ${}^8\text{B}$  neutrino spectrum is shown with the corresponding yearly averaged survival probabilities, computed without taking into account the regeneration in the Earth, which represents a small effect for our purposes [29]. It is worth nothing that the minimum probability in the SMA solution occurs in the  ${}^7\text{Be}$  energy region. The consequent spectral distortions are shown in Fig. 7.

Possible scenarios include also the existence of sterile neutrino oscillations with  $\sin^2 2\theta$ ,  $\Delta m^2$  similar to those corresponding to SMA for standard neutrinos but no LMA solution [30].

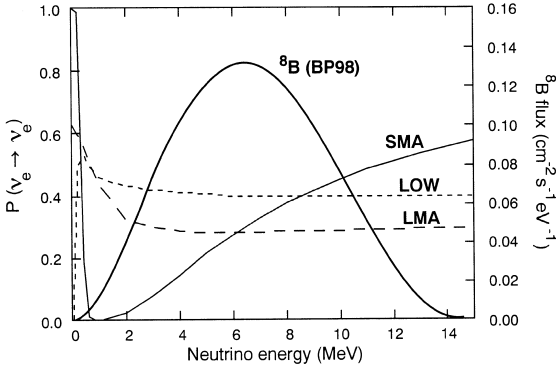


Fig. 6. The  $^8\text{B}$  flux (right scale) is compared on the same energy scale with the average survival probabilities (left scale) for various MSW solutions.

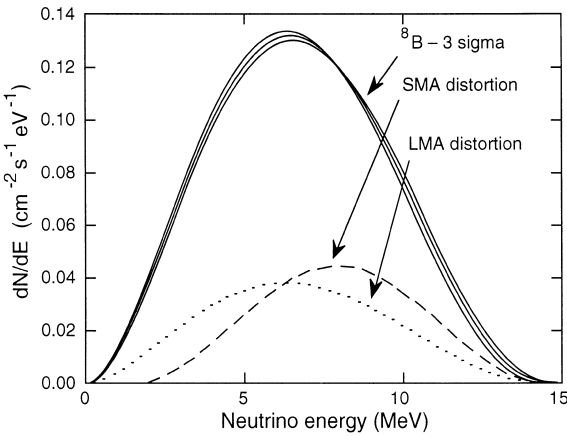


Fig. 7. The spectral distortion due to the MSW effect is shown with BP98 undistorted  $^8\text{B}$  flux.

A possible way to combine the ICARUS measurements from the two independent detection channels, elastic scattering and absorption events (Gamow–Teller and Fermi), is to compute the following ratio:

$$R = \frac{N^{\text{ES}}/N_0^{\text{ES}}}{\frac{1}{2}(N^{\text{GT}}/N_0^{\text{GT}} + N^{\text{FT}}/N_0^{\text{FT}})} \quad (1)$$

where  $N^{\text{ES}}$ ,  $N^{\text{GT}}$ ,  $N^{\text{FT}}$  are the measured event rates (elastic, Gamow–Teller and pure Fermi, respectively), and  $N_0^{\text{ES}}$ ,  $N_0^{\text{GT}}$ ,  $N_0^{\text{FT}}$  are the predicted event rates in the case of standard neutrino without oscillations.

The proposed ratio is an indicator with the following advantages:

- it is independent of the  $^8\text{B}$  total neutrino flux, predicted by different solar models, and of any possible pure astrophysical suppression factor;
- it does not depend on experimental threshold energies or on the adopted cross-section files for the different channels.

The above introduced quantities are defined as follows:

$$N^{\text{ES}} = \Phi_{^8\text{B}}^{\text{SM}} \int_{E_{\nu,\text{min}}}^{+\infty} dE_{\nu} S(E_{\nu}) \times [\sigma_{\nu_e}^{\text{ES}}(E_{\nu}) P(E_{\nu}) + \sigma_{\nu_{\mu(\tau)}}^{\text{ES}}(E_{\nu}) (1 - P(E_{\nu}))] \quad (2)$$

where  $E_{\nu}$  is the neutrino energy,  $S(E_{\nu})$  is the standard  $^8\text{B}$  neutrino spectrum,  $\sigma_{\nu_e}^{\text{ES}}(E_{\nu})$  is the elastic scattering cross-section for electron-neutrinos while  $\sigma_{\nu_{\mu(\tau)}}^{\text{el}}(E_{\nu})$  is the corresponding cross-section for mu-neutrinos or tau-neutrinos and  $P(E_{\nu})$  is the survival probability for  $\nu_e \rightarrow \nu_{\mu(\tau)}$  or  $\nu_e \rightarrow \nu_s$  transitions. In the second case the contribution has to be omitted. These probabilities are a function of neutrino parameters  $\Delta m^2$  and  $\sin^2 2\theta$ . The lower limit in the integral is

$$E_{\nu,\text{min}} = \frac{1}{2} [T_{\text{th}} + \sqrt{T_{\text{th}}^2 + 2T_{\text{th}}m_e}] \quad (3)$$

where  $T_{\text{th}}$  is the electron threshold kinetic energy and  $m_e$  is the electron mass.

For Gamow–Teller and Fermi transitions the corresponding event rates are defined as

$$N^{\text{GT}} = \Phi_{^8\text{B}}^{\text{SM}} \int_{E_{\nu,\text{min}}^{\text{GT}}}^{+\infty} dE_{\nu} S(E_{\nu}) \sigma^{\text{GT}}(E_{\nu}) P(E_{\nu}) \quad (4)$$

where

$$E_{\nu,\text{min}}^{\text{GT}} = T_{\text{th}} + 1.50 \text{ MeV} + 2.29 \text{ MeV}$$

and

$$N^{\text{FT}} = \Phi_{^8\text{B}}^{\text{SM}} \int_{E_{\nu,\text{min}}^{\text{F}}}^{+\infty} dE_{\nu} S(E_{\nu}) \sigma^{\text{FT}}(E_{\nu}) P(E_{\nu}) \quad (5)$$

where

$$E_{\nu,\text{min}}^{\text{F}} = T_{\text{th}} + 1.50 \text{ MeV} + 4.38 \text{ MeV}.$$

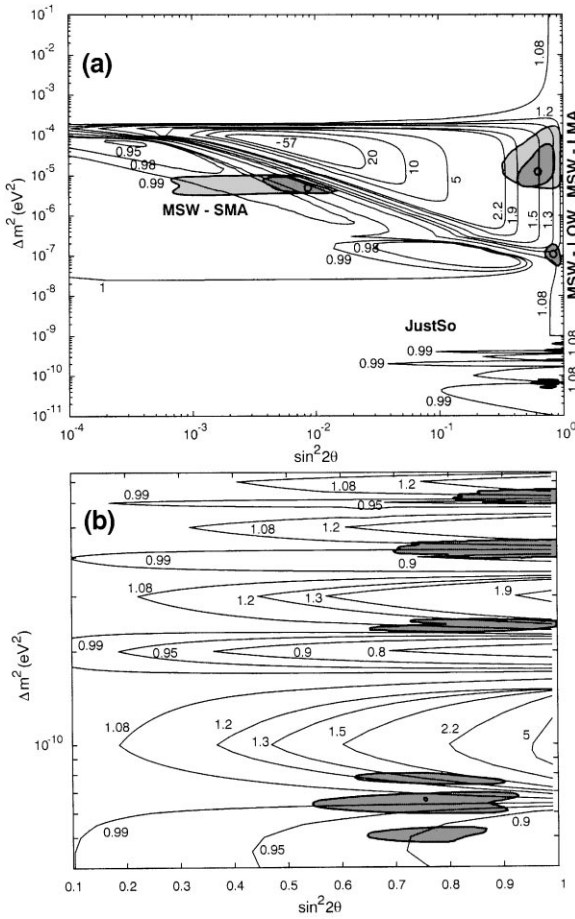


Fig. 8. Iso- $R$  curves for active neutrinos. (b) is a blow up of the lower part of (a).

The corresponding standard neutrino event rates ( $N_0^{ES}, N_0^{GT}, N_0^{FT}$ ) may be obtained from the previous formulae putting  $P(E_\nu) \equiv 1$ .

The iso- $R$  curves obtained from Monte Carlo simulation, taking into account the neutrino oscillation, are shown in Figs. 8 and 9 which refer to active and sterile neutrinos, respectively.

As usual the shaded regions represent the allowed regions resulting from five solar neutrino experiments (Homestake-chlorine, Kamiokande, GALLEX, SAGE, and Super-Kamiokande) for 90% and 95% confidence level. From the figures we can deduce the solutions of the SNP which the ICARUS experiment will be able to probe. These solutions together with the  $R$ -ratio range, the level

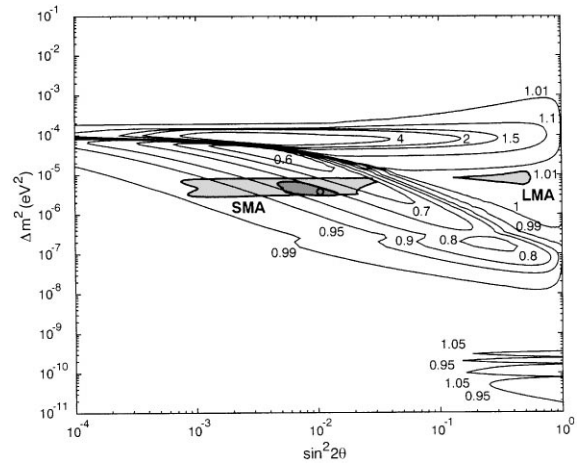


Fig. 9. Iso- $R$  curves for sterile neutrinos.

of exclusion, and the minimal exposure time for one module (years) are reported in detail in Table 9.

There are combinations of neutrino parameters for which  $R = 1$ , despite the MSW effect takes place in the sun. Such regions cannot be excluded by this method and represent its theoretical limit. The experimental limit is given by the ICARUS ability to detect a small deviation from  $R = 1$ , which is related to the statistical error and all the experimental systematic error sources.

Taking into account only the statistical error and the rates foreseen in Section 4, we estimate the one-sigma relative uncertainty for  $R$  as a function of the exposure time for one module. The results are displayed in Table 10.

From the two tables above it is possible to say that at the one-sigma level one module for one year will be able to test the Active MSW-LOW solution. Similar predictions for the other solutions are reported in the last column of Table 9.

From the results above it is clear that it will be possible to test the Active MSW-SMA solution to the SNP with this method using one module for three years, but there is a reasonable hope to test the largest part of all the other regions in a shorter period. Finally it has to be recalled that the spectral methods are much more sensitive than the  $R$ -ratio method and that they are better suited to testing the Active MSW-SMA region.

Table 9

The  $R$ -ratio range, the level of exclusion and the minimal exposure time for one module-year

Solution region	$R$	Exclusion level	Minimal exposure (one module-year)
Active MSW-SMA	1.0–1.1	Nearly complete	4
Active MSW Extended SMA	1.1–1.3	Only the largest mixing side	> 1
Active MSW-LOW	1.1–1.3	Complete	> 1
Active MSW-LMA	1.3–1.9	Complete	1
Active MSW Extended LMA	1.2–2.3	Complete	1
Active JustSo	0.8–1.0	Partial	> 1
Active JustSo	1.0–2.0	Partial	> 1
Sterile MSW-SMA	0.8–0.9	Complete	1
Sterile MSW Extended SMA	0.6–0.8	All the higher mixing angle side	1
Sterile MSW Extended SMA	0.6–1.0	Complete	> 1

Table 10

The one-sigma relative uncertainty for  $R$  as a function of the years of exposure time, together with the limits of the one-sigma exclusion region

Exposure	$\Delta R/R\%$	$R_{\min}$	$R_{\max}$
1	10.6	0.89	1.11
2	7.5	0.92	1.08
4	5.3	0.95	1.05
8	3.8	0.96	1.04

## References

- [1] B.T. Cleveland et al., *Astrophys. J.* 496 (1998) 505.
- [2] Y. Fukuda et al. (Kamiokande Collaboration), *Phys. Rev. Lett.* 77 (1996) 1683.
- [3] P. Anselmann et al. (GALLEX collaboration), *Phys. Lett. B* 342 (1995) 440.
- [4] J.N. Abdurashitov et al. (SAGE Collaboration), *Phys. Lett. B* 328 (1994) 234.
- [5] Y. Suzuki, (Super-Kamiokande Collaboration), *Nucl. Phys. B (Proc. Suppl.)* 77 (1999) 35.
- [6] J.N. Bahcall, S. Basu, M.H. Pinsonneault, *Phys. Lett. B* 433 (1998) 1.
- [7] J.N. Bahcall, P.I. Krastev, A.Yu. Smirnov, *Phys. Rev. D* 58 (1998) 096016.
- [8] J.N. Bahcall, P.I. Krastev, *Phys. Rev. B* 436 (1998) 243.
- [9] M. Apollonio et al. (CHOOZ collaboration), *Phys. Lett. B* 420 (1998) 397.
- [10] P. Cennini et al. (ICARUS Collaboration), A first 600 ton ICARUS detector installed at the Gran Sasso Laboratory, addendum to Proposal and LNGS Report LNGS-94/99 I & II, May 1995.
- [11] R. Dolfini et al., Study of solar neutrino detection in the 600 ton liquid argon ICARUS time projection chamber, LNGS Report LNGS-97/49, 1997.
- [12] W. Trinder et al., *Phys. Lett. B* 415 (1997) 211.
- [13] F. Arneodo et al., *Il Nuovo Cimento A* 8 (1999) 819.
- [14] R. Brun, F. Bruyant, M. Maire, A.C. Mc Pherson, P. Zanarini, GEANT 3, CERN Report DD/EE/84-1, September 1987.
- [15] MCNP – A general Monte Carlo code for neutron and photon transport, Version 4.2, Los Alamos National Laboratory Report LA7396-M, revised April 1991.
- [16] A. Fassò, A. Ferrari, J. Ranft, P. Sala, FLUKA: present status and future development, Proceedings of the Fourth International Conference on Calorimetry in High Energy Physics, La Biodola, Italy, 21–26 September 1993, World Scientific, Singapore, 1994.
- [17] F. Arneodo et al., The ICARUS 50 l LAr TPC in the CERN  $\nu$  Beam, Proceedings of 36th Workshop on New Detectors, Erice, Italy, 1–7 November 1997, World Scientific, Singapore, 1999, p. 3.

- [18] E. Bellotti, Nuclear Physics at Gran Sasso, Nucl. Phys. News I (3) (1991) 18.
- [19] C.D. Hodgman, R.C. Weast, S.N. Selby (Eds.), CRC Handbook of Chemistry and Physics, 46th Edition, 1965.
- [20] A. Esposito, Misure di radioattività nei campioni di materiale da utilizzare per strutture interne del LNGS dell'INFN, LNF Report LNF-86/60, 1986 (in Italian).
- [21] R. Vandenbosch, J.R. Huizenga, Nuclear Fission, Academic Press, New York, 1973.
- [22] J.B. Marion, J.L. Fowler, Fast neutron Physics, Interscience Publishers, New York, 1960.
- [23] P. Cennini et al., On atmospheric  $^{39}\text{Ar}$  and  $^{42}\text{Ar}$  abundance, Nucl. Instr. and Meth. A 356 (1994) 256.
- [24] ICARUS Collaboration, ICARUS II: second generation proton decay experiment and neutrino observatory at the Gran Sasso Laboratory, LNGS Report LNGS-94/99, Vol. 1, 1994, p. 84.
- [25] A. Somigliana, Misure di contaminazioni radioattive bassissime in materiali per schermature con particolare riferimento a piombo antico e moderno, Degree Thesis, Università degli Studi di Milano, 1989/90 (in Italian).
- [26] W.E. Ormand et al., Phys. Lett. B 345 (1995) 343.
- [27] J.N. Bahcall, Neutrino Astrophysics, Cambridge University Press, Cambridge, 1989.
- [28] W. Liu et al., Z. Phys. A 359 (1997) 1.
- [29] M. Maris, Variabilità temporale del flusso di neutrini solari in rivelatori sotterranei, Ph.D. Thesis, Dipartimento di Fisica Nucleare e Teorica, Pavia University, 1996 (in Italian).
- [30] M. Maris, S.T. Petcov, Phys. Rev. D 58 (1998) 113008.